Electric sail phasing maneuvers for constellation deployment

L. Niccolai*, A. Caruso†, A. A. Quarta‡, and G. Mengali§
Department of Civil and Industrial Engineering, University of Pisa, Italy, I-56122

The aim of this work is to investigate heliocentric phasing maneuvers performed by a spacecraft propelled by an Electric Solar Wind Sail, an innovative propellantless propulsion system. It is assumed that the sail may be controlled by varying its attitude, and by switching the tether grid off to obtain Keplerian arcs in the trajectory. The analysis is conducted within an optimal framework, whose aim is to find the minimum-time phasing trajectory for a given angular drift, and the corresponding time variation of the control variables. A typical phasing scenario is analyzed, by considering either a drift ahead or a drift behind maneuver option. We also investigate the possibility of using an Electric Solar Wind Sail-based deployer to place a constellation of satellites on the same heliocentric circular orbit. The corresponding flight times are obtained as a function of the sail performance and the number of satellites.

Nomenclature

$\boldsymbol{a}$	=	propulsive acceleration vector, [mm/s^2]
a_c	=	characteristic acceleration, [mm/s^2]
a_r, a_θ	=	propulsive acceleration components, [mm/s^2]
$\mathcal{H}$	=	Hamiltonian function
J	=	performance index
m_{pay}	=	payload mass, [kg]
m_{tot}	=	total mass, [kg]
N	=	number of satellites
$\hat{\boldsymbol{n}}$	=	normal unit vector
$\hat{\boldsymbol{r}}$	=	radial unit vector
r	=	Sun-spacecraft distance, [au]
$r_\oplus$	=	Sun-Earth distance (1 au)
t	=	time instant, [TU]
u, v	=	spacecraft velocity components, [au/DU]
$\boldsymbol{v}$	=	spacecraft orbital velocity vector, [au/TU]
α_n	=	pitch angle, [deg]
α_p	=	primer vector angle, [deg]
$\Delta\phi$	=	angular drift, [deg]
θ	=	angular coordinate, [deg]
λ_r, λ_θ, λ_u, λ_v	=	adjoint variables
$\mu_\odot$	=	Sun's gravitational parameter, [au^3/TU^2]
τ	=	switching parameter
ω	=	angular velocity, [TU^{-1}]

Subscripts

0	=	initial time instant
A	=	drift ahead
B	=	drift behind

*Research assistant, Department of Civil and Industrial Engineering, University of Pisa, Via Caruso 8, Pisa, Italy, lorenzo.niccolai@ing.unipi.it
†Ph.D. student, Department of Civil and Industrial Engineering, University of Pisa, Via Caruso 8, Pisa, Italy, andrea.caruso@ing.unipi.it
‡Professor, Department of Civil and Industrial Engineering, University of Pisa, Via Caruso 8, Pisa, Italy, a.quarta@ing.unipi.it
§Professor, Department of Civil and Industrial Engineering, University of Pisa, Via Caruso 8, Pisa, Italy, g.mengali@ing.unipi.it

f = final time instant
i = i-th trajectory arc
max = maximum
tr = threshold value

Superscripts

$\cdot$ = time derivative
$-$ = design value
$\star$ = optimal

1. Introduction

Since the dawn of space exploration, the study of the Sun and the main properties of the heliosphere have much attracted the interest of the scientific community. The first and more obvious reason is that some catastrophic solar events, such as coronal mass ejections (CMEs), could cause damages on orbiting spacecraft and eventually induce communication problems on the Earth. It is therefore important to guarantee the possibility of obtaining an early warning of such events. Moreover, a deeper understanding of the solar behaviour could increase our knowledge of other Sun-related phenomena, such as solar irradiance cycles and solar wind properties, which have a high impact on Earth environment and climate, and on operating satellites. The first mission totally dedicated to the scientific investigation of the Sun's characteristics was Helios 1 [1], which provided relevant data on the solar wind and the corona. In 1980, NASA launched the Solar Maximum Mission [2], aimed at studying solar flares and high-energy components of the Sun's spectrum during its solar maximum, and a similar investigation was later conducted by the Japanese mission Yohkoh [3], launched in 1991. The lack of information about high-latitude solar zones was an important motivation for the Ulysses mission [4], which collected important data on the polar regions of the Sun [5].

More recently, three satellites have been placed in the vicinity of the L_1 collinear Lagrangian point of the Sun-Earth gravitational field [6]. NASA's Advanced Composition Explorer [7] is orbiting on a small-amplitude Lissajous orbit and is devoted to the study of solar wind and cosmic rays, whereas the WIND [8] mission is concentrated on the solar wind. Finally, the Solar and Heliospheric Observatory (SOHO) [9], a joint mission between ESA and NASA, is tracking a Halo orbit around L_1 and is equipped with several scientific instruments, aimed at analyzing the solar surface and atmosphere, the corona, and the solar wind. In this context, the use of a propellantless propulsion system could allow an artificial Lagrangian (L_1-type) point closer to the Sun to be generated [10–12].

The most recent Sun-focused mission is the NASA's Parker Solar Probe [13], launched in August 2018, which will perform three close passages to the Sun, but a potentially revolutionary new approach for solar scientific investigations has been tested by the Solar Terrestrial Relations Observatory (STEREO) mission [14], launched in 2006 and operative until 2016. STEREO was made of two twin spacecraft, one drifting ahead of the Earth and one behind it, thus providing three-dimensional stereoscopic images of the Sun. The angular drift of the two satellites was obtained thanks to a slightly different semimajor axis of their orbits, but a similar result could likewise be obtained by means of a heliocentric phasing maneuver, which could be performed by a spacecraft equipped with a propellantless propulsion system [15, 16].

The aim of this paper is to investigate the performance of the Electric Solar Wind Sail (or E-sail) [17], a recent propellantless propulsion system, in a heliocentric phasing mission scenario. In particular, the objective is to extend previous preliminary results [16], by means of the thrust model suggested by Huo et al. [18]. The analysis of a phasing maneuver can be addressed with two different strategies. The first one involves the Hill-Clohessy-Wiltshire equations [19], which are valid as long as the distance between the instantaneous position of the spacecraft and that of the reference (working) orbit is sufficiently small. The integration of these equations provides a set of analytical expressions that give the spacecraft position as a function of time [20], so that the required maneuver time and the angular displacement can be calculated once the E-sail (fixed) attitude is chosen. However, such an approach has two important intrinsic limitations. First, its accuracy is limited by the assumption that the spacecraft remains close to the initial heliocentric orbit. Moreover, it does not permit a variation of the E-sail attitude to be considered and, for that reason, the resultant trajectories could be quite different from an optimal solution.

Accordingly, in this work phasing maneuvers are analyzed within an optimal approach, by minimizing the required flight time [21] and using the nonlinear equations of motion in a heliocentric framework. In particular, the optimal control law of the E-sail attitude and the corresponding minimum maneuver time are obtained by means of an indirect

approach. The system performance is analyzed within two different mission cases, that is, either a conventional heliocentric phasing maneuver, or the deployment of a constellation of equally-spaced spacecraft on the same (circular) heliocentric orbit. Both scenarios are discussed in the next section.

2. Problem description

A heliocentric phasing maneuver consists in varying the angular position of a spacecraft along its orbit, without affecting the other orbital parameters [22, 23]. Phasing trajectories are usually classified into drift ahead or drift behind maneuvers. In the former (latter) case, the final spacecraft angular coordinate is greater (smaller) than that of a virtual point which tracks its initial heliocentric orbit. The two previous cases are both shown in Fig 1, which illustrates a drift ahead (or behind) maneuver with respect to the Earth, assuming that the spacecraft leaves the Earth's sphere of influence with zero excess velocity relative to it.

A phasing trajectory may be obtained in a very simple way, with a bi-impulsive maneuver by means of a chemical thruster, in which the two impulses give the same velocity variation and are both tangentially directed. This approach, however, usually requires a large amount of propellant consumption. Therefore, the possibility of exploiting a low-thrust propellantless propulsion system for such purpose is an interesting option. In particular, the problem of investigating a solar sail-enabled phasing maneuver has been investigated at length in the literature [15, 24, 25], with possible applications involving a Smart Dust [20, 26], a miniaturized femtosatellite with a high area-to-mass ratio [27]. Some results exist also for a spacecraft propelled by an E-sail [16], even though they are based on a quite simplified thrust model.

A special applications of (consecutive) phasing maneuvers consists in a constellation deployment by means of a "deployer" spacecraft. Such a mission involves an E-sail-based deployer whose payload is constituted by $N \geq 2$ small satellites, each one being equipped with a suitable scientific instrumentation. The constellation deployment is achieved by means of succeeding heliocentric phasing maneuvers. In particular, at the end of each phasing trajectory arc, one of the satellites stowed in the deployer is ejected (with zero velocity relative to it). Once the whole payload has been ejected from the deployer, the deployment phase ends, and the satellites are all placed on the same heliocentric orbit with a prescribed angular separation, thus enabling a scientific observation of the Sun by different locations. Such an idea may be considered as an important extension of the STEREO mission concept [14].

3. Mathematical model

According to the recent results by Huo et al. [18], the propulsive acceleration vector $\boldsymbol{a}$ generated by an E-sail may be written as

$$\boldsymbol{a} = \tau \, \frac{a_c}{2} \left(\frac{r_\oplus}{r} \right) \left[\hat{\boldsymbol{r}} + (\hat{\boldsymbol{r}} \cdot \hat{\boldsymbol{n}}) \right] \tag{1}$$

where τ is a switching parameter that accounts for the possibility of switching either on ($\tau = 1$) or off ($\tau = 0$) the electron gun that maintains the E-sail grid voltage, $r_\oplus \triangleq 1$ au is the Sun-Earth distance, $\hat{\boldsymbol{r}}$ is the Sun-spacecraft unit vector (with $r = \|\boldsymbol{r}\|$), and $\hat{\boldsymbol{n}}$ is the unit vector normal to the E-sail plane and directed outwards with respect to the Sun; see Fig. 2. In Eq. (1), a_c is the characteristic acceleration, which depends on the grid voltage and the sail design parameters, and is usually chosen as the reference performance parameter for an E-sail. The assumption of constant value of a_c implies that the variations of the solar wind properties are neglected to a first order. The interested reader may find more details on this topic in Refs. [28, 29]. Equation (1) also assumes that the E-sail tethers belong to same plane (that is, the E-sail has a perfectly flat shape), in accordance with the recent results stating that the thrust magnitude reduction due to tether inflection is negligible [30–32]. Note that the thrust model of Eq. (1) gives a propulsive acceleration vector $\boldsymbol{a}$ whose maximum inclination with respect to the radial direction is about 19.5 deg.

Assume now that a spacecraft propelled by an E-sail is covering a circular heliocentric orbit of radius r_0, and its thrust belongs to the orbital plane. Let $\mathcal{T}(O; r, \theta)$ be a polar heliocentric reference frame, where θ is an angular coordinate measured counterclockwise from a generic fixed direction. In a two-dimensional motion, the radial (a_r) and

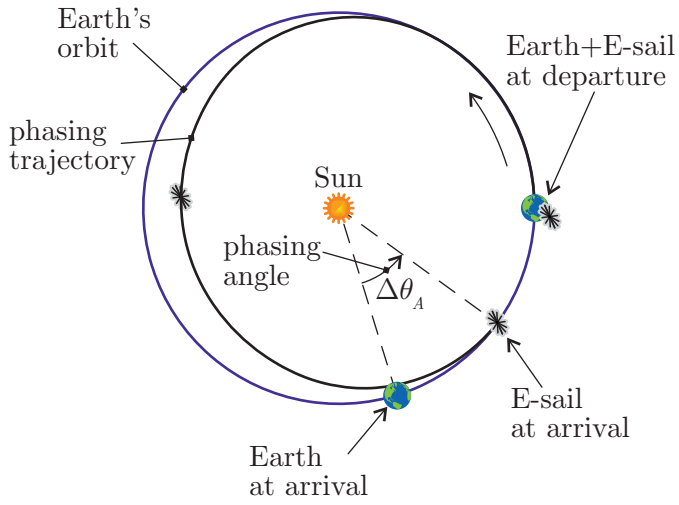

(a) Drift ahead

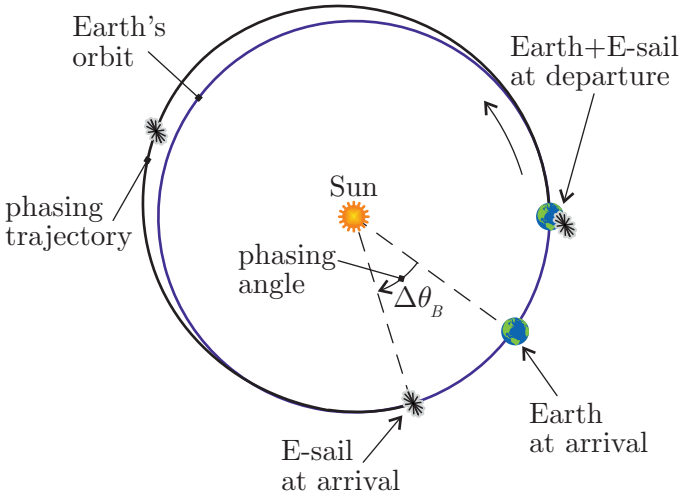

(b) Drift behind

Figure 1. Conceptual sketch of a phasing maneuver on Earth's heliocentric orbit starting from the Earth's position.

circumferential (a_θ) components of the propulsive acceleration may be written as (see Eq. (1))

$$a_r = \tau \frac{a_c}{4} \left(\frac{r_\oplus}{r}\right) [3 + \cos(2\,\alpha_n)] \tag{2}$$

$$a_\theta = \tau \frac{a_c}{4} \left(\frac{r_\oplus}{r}\right) \sin(2\,\alpha_n) \tag{3}$$

where the pitch angle $\alpha_n \in [-90, 90]$ deg denotes the angle between $\hat{\boldsymbol{r}}$ and $\hat{\boldsymbol{n}}$, and is defined as

$$\alpha_n \triangleq \text{sign}(\boldsymbol{v} \cdot \hat{\boldsymbol{n}}) \arccos(\hat{\boldsymbol{r}} \cdot \hat{\boldsymbol{n}}) \tag{4}$$

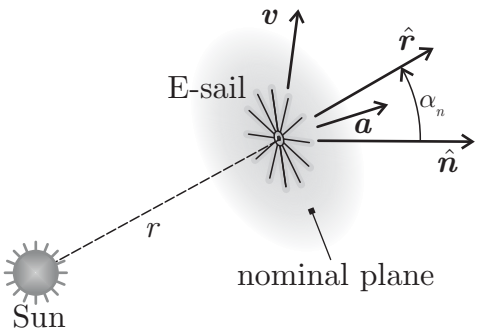

Figure 2. Conceptual sketch of the vectors involved in E-sail thrust generation. Adapted from Ref. [28]

where $\boldsymbol{v}$ is the spacecraft velocity vector. Using Eqs. (2) and (3), the spacecraft dynamics may be written in $\mathcal{T}$ as follows

$$\dot{r} = u \tag{5}$$

$$\dot{\theta} = v/r \tag{6}$$

$$\dot{u} = -\frac{\mu_\odot}{r^2} + \frac{v^2}{r} + \tau\,\frac{a_c}{4}\,\left(\frac{r_\oplus}{r}\right)\,[3 + \cos(2\,\alpha_n)] \tag{7}$$

$$\dot{v} = -\frac{u\,v}{r} + \tau\,\frac{a_c}{4}\,\left(\frac{r_\oplus}{r}\right)\,\sin(2\,\alpha_n) \tag{8}$$

where the dot symbol denotes a time derivative, $\mu_\odot$ is the Sun's gravitational parameter, u and v are the radial and tangential component of the spacecraft velocity vector $\boldsymbol{v}$. According to Eqs. (5)–(8), the system dynamics is described by the four state variables $[r,\,\theta,\,u,\,v]$ and the two control variables $[\tau,\,\alpha_n]$.

3.1 Trajectory optimization

Let the state variables at the initial time $t_0 \triangleq 0$ be

$$r(t_0) = r_0, \quad \theta(t_0) = 0, \quad u(t_0) = 0, \quad v(t_0) = \sqrt{\mu_\odot/r_0} \tag{9}$$

where the angular coordinate has been chosen arbitrarily, without loss of generality, because the reference orbit is circular. The optimization of a phasing maneuver consists in looking for the control law that minimizes the time $\Delta t \triangleq t_f - t_0$ required for the spacecraft to track the same initial orbit, but with an angular drift $\Delta\phi \in [0,\,360)\,\mathrm{deg}$, measured counterclockwise from the Sun-spacecraft line at t_f. In other terms, the boundary conditions at t_f are given by

$$r(t_f) = r_0, \quad \theta(t_f) = t_f\,\omega_0 + \Delta\phi, \quad u(t_f) = 0, \quad v(t_f) = \sqrt{\mu_\odot/r_0} \tag{10}$$

where $\omega_0 \triangleq \sqrt{\mu_\odot/r_0^3}$ is the angular velocity on the reference orbit. Denoting with $\Delta\theta_A$ or $\Delta\theta_B$ the absolute value of the angular variation in a drift ahead or a drift behind maneuver, respectively, $\Delta\phi$ is defined as

$$\Delta\phi \triangleq \begin{cases} \Delta\theta_A & \text{drift ahead case} \\ 360\,\mathrm{deg} - \Delta\theta_B & \text{drift behind case} \end{cases} \tag{11}$$

in accordance with Fig. 1.

The minimum-time trajectory corresponding to the phasing maneuver with boundary conditions (9) and (10), is obtained by maximizing the performance index

$$J \triangleq -t_f \tag{12}$$

The dynamical system defined by Eqs. (5)–(8) admits an Hamiltonian function $\mathcal{H}$, defined as

$$\mathcal{H} \triangleq \lambda_r\, u + \lambda_\theta\, \frac{v}{r} + \lambda_u \left(-\frac{\mu_\odot}{r^2} + \frac{v^2}{r} + a_r \right) + \lambda_v \left(-\frac{u\, v}{r} + a_\theta \right) \tag{13}$$

where a_r and a_θ are given by Eqs. (2) and (3), while λ_r, λ_θ, λ_u, and λ_v denote the adjoint variables associated with the state variables r, θ, u, and v. Their time derivatives are given by the Euler-Lagrange equations as

$$\dot{\lambda}_r \triangleq -\frac{\partial \mathcal{H}}{\partial r} = \lambda_\theta\, \frac{v}{r^2} + \lambda_u \left(\frac{v^2}{r^2} - \frac{2\,\mu_\odot}{r^3} + \frac{a_r}{r} \right) + \lambda_v \left(-\frac{u\, v}{r^2} + \frac{a_\theta}{r} \right) \tag{14}$$

$$\dot{\lambda}_\theta \triangleq -\frac{\partial \mathcal{H}}{\partial \theta} = 0 \tag{15}$$

$$\dot{\lambda}_u \triangleq -\frac{\partial \mathcal{H}}{\partial u} = -\lambda_r + \lambda_v\, \frac{v}{r} \tag{16}$$

$$\dot{\lambda}_v \triangleq -\frac{\partial \mathcal{H}}{\partial v} = -\lambda_\theta\, \frac{1}{r} - 2\,\lambda_u\, \frac{v}{r} + \lambda_v\, \frac{u}{r} \tag{17}$$

In particular, Eq. (15) states that λ_θ is a constant of motion.

The optimal phasing trajectory is the solution of a two-point boundary value problem (TPBVP), constituted by the equations of motion (5)–(8) and the Euler-Lagrange equations (14)–(17), with four boundary conditions at $t = t_0$ (Eqs. (9)) and four at $t = t_f$ (Eqs. (10)). The final time t_f is obtained by enforcing the transversality condition [33], which is written from Eq. (12) and the second of Eqs. (10) as

$$\mathcal{H}(t_f) = 1 + \lambda_\theta \sqrt{\frac{\mu_\odot}{r_0^3}} \tag{18}$$

Using the Pontryagin's maximum principle, the optimal control variables $[\tau^*,\ \alpha_n^*]$ at each time instant t are found by maximizing the Hamiltonian function given by Eq. (13). According to the results by Huo et al. [18], the optimal control law is given by

$$\tau^* = \frac{1 + \operatorname{sign}\left(1 + 3\,\cos\alpha_p\right)}{2} \tag{19}$$

$$\alpha_n^* = \frac{\alpha_p}{2} \tag{20}$$

where the angle $\alpha_p \in [-180, 180]\,\mathrm{deg}$, defined as

$$\alpha_p \triangleq \operatorname{sign}(\lambda_v)\, \arccos\left(\frac{\lambda_u}{\sqrt{{\lambda_u}^2 + {\lambda_v}^2}} \right) \tag{21}$$

denotes the angle between the Lawden's primer vector [34] $\boldsymbol{\lambda_v} \triangleq [\lambda_u,\ \lambda_v]^{\mathrm{T}}$ and the radial unit vector $\hat{\boldsymbol{r}}$.

4. Numerical simulations

The time-optimal phasing maneuvers performed by an E-sail have been investigated with numerical simulations, in which the differential equations of the TPBVP have been integrated in double precision by means of a variable order Adams-Bashforth-Moulton solver scheme [35, 36] with absolute and relative errors of 10^{-12}.

4.1 Phasing maneuvers

As a first exemplary case, consider a spacecraft propelled by an E-sail with characteristic acceleration $a_c = 0.1\,\mathrm{mm/s^2}$. The reference orbit coincides with the Earth's (circular) heliocentric orbit ($r_0 = r_\oplus$). This case corresponds to a situation

in which the spacecraft leaves the planet's sphere of influence with zero excess velocity. Figure 3 shows the minimum flight time t_f as a function of the angular drift $\Delta\phi$ given by Eq. (11), in both cases of either drift ahead or drift behind maneuvers.

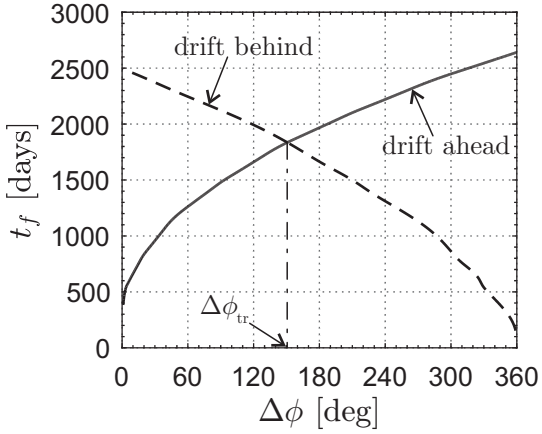

Figure 3. Minimum flight time t_f as a function of the angular drift $\Delta\phi$ when $a_c = 0.1\,\mathrm{mm/s^2}$.

Each value of $\Delta\phi$ can be obtained, in principle, both with a drift ahead and a drift behind maneuver. When only the magnitude of the angular drift is relevant for the mission requirements, considering either a drift ahead maneuver with angular change $\Delta\overline{\theta}_A$ or a drift behind maneuver with $\Delta\overline{\theta}_B = \Delta\overline{\theta}_A$, the latter choice is better in terms of flight time. However, when a given angular displacement $\Delta\phi$ must be obtained (see Eq. (11)), a drift ahead maneuver could be more convenient, in particular for small values of $\Delta\phi$. There exists, however, a threshold value, beyond which a drift behind maneuver requires a smaller flight time. This is clearly illustrated in Fig. 3, from which the value of $\Delta\phi_{\rm tr}$ is about 150.7 deg. The global minimum of the flight time, for both cases of drift ahead and drift behind maneuvers, is reported in Figure 4 as a function of $\Delta\phi$. The maximum flight time is obtained when $\Delta\phi = \Delta\phi_{\rm tr}$ and is equal to $t_{f_{\rm max}} = 1836\,\mathrm{days} \simeq 5\,\mathrm{years}$.

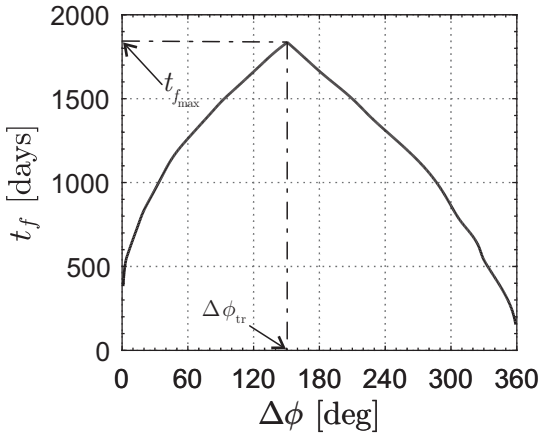

Figure 4. Global minimum of the flight time t_f as a function of the angular drift $\Delta\phi$ when $a_c = 0.1\,\mathrm{mm/s^2}$.

4.2 Constellation deployment scenario

The constellation deployment scenario has been described in Section 2. The deployer has a total payload mass $m_{\rm pay} = 100\,\mathrm{kg}$, which coincides with the total mass of the N spacecraft stowed within it, and is propelled by an E-sail

with (initial) characteristic acceleration $a_c = \{0.1,\ 1\}\,\mathrm{mm/s^2}$. According to the E-sail mass budget model of Ref. [37], these performance parameters could be achieved by a spacecraft with a total in-flight mass of $m_{\mathrm{tot}} = \{280,\ 391\}\,\mathrm{kg}$. The constellation deployment can be seen as a succession of consecutive phasing maneuvers with the same angular drift and with identical boundary conditions as those of Eqs. (9) and (10). This is a consequence of the assumption that the reference orbit is circular, so that the initial value of the angular coordinate may be freely chosen.

Assuming that the first satellite is released in proximity of Earth (just outside its sphere of influence), the trajectory tracked by the deployer is composed of $N-1$ arcs. The angular drift in each arc depends on the number N of satellites stowed in the deployer. Indeed, if a constellation with equally-spaced elements must be obtained, the angular drift in the generic i-th trajectory arc is

$$\Delta\theta_{B_i} = \frac{360}{N}\,\mathrm{deg} \qquad \text{for } i = 1, 2, \ldots, N-1 \tag{22}$$

where a drift behind maneuver is assumed, based on the previously discussed results. The value of $\Delta\phi_i$ is obtained by substituting Eq. (22) into Eq. (11). The E-sail characteristic acceleration has a discontinuity at each deployment time t_{fi}, due to the instantaneous reduction of the total deployer mass. The characteristic acceleration a_{c_i} during the i-th trajectory arc is

$$a_{c_i} = a_{c_{i-1}}\,\frac{m_{\mathrm{tot}}}{m_{\mathrm{tot}} - m_{\mathrm{pay}}(i/N)} \qquad \text{for } i = 1, 2, \ldots, N-1 \tag{23}$$

where $a_{c_0} = a_c$ is the initial characteristic acceleration. The total maneuver time is simply the sum of all the time intervals required to perform each phasing maneuver, viz.

$$t_f = \sum_{i=1}^{N-1} t_{f_i} \tag{24}$$

Figure 5 shows the values of t_{f_i} as a function of the (initial) characteristic acceleration a_c and the total number of satellites N. Once the E-sail characteristic acceleration in the i-th arc is found with Eq. (23), the flight time t_{f_i} is obtained graphically from Fig. 5 as a function of N. Finally, the total time for the constellation deployment is given by Eq. (24). Table 1 summarizes the results for an E-sail-based constellation deployment for different numbers of satellites N, assuming an initial characteristic acceleration $a_c = 0.1\,\mathrm{mm/s^2}$

Table 1. Constellation deployment performance as a function of N when $a_c = 0.1\,\mathrm{mm/s^2}$.

$\Delta\theta_{B_i}$ [deg]	N	t_f [days]
120	3	2385
90	4	3012
72	5	3428
60	6	3799
40	9	4685
30	12	5315

The deployment of a considerable number of satellites requires a very high value of t_f. Indeed, even assuming that the deployer contains just three satellites (i.e. $N = 3$), the total deployment time amounts to more than 6 years. However, the mission time could be substantially shortened by increasing the E-sail performance. This is clearly illustrated in Tab. 2, which reports the same cases as those of Tab. 1, but now assuming $a_c = 1\,\mathrm{mm/s^2}$.

For example, if the deployer inserts $N = 3$ equally-spaced spacecraft on the reference orbit (i.e. $\Delta\theta_{B_i} = 120\,\mathrm{deg}$), the total mission time reduces to 785 days $\simeq 2.15$ years. The corresponding trajectory is sketched in Fig. 6, which shows that the optimal transfer trajectory includes also coasting (Keplerian) arcs, in which $\tau = 0$.

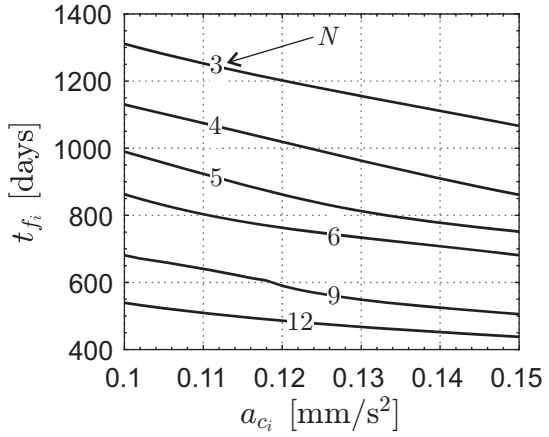

(a) $a_c = 0.1\,\mathrm{mm/s^2}$

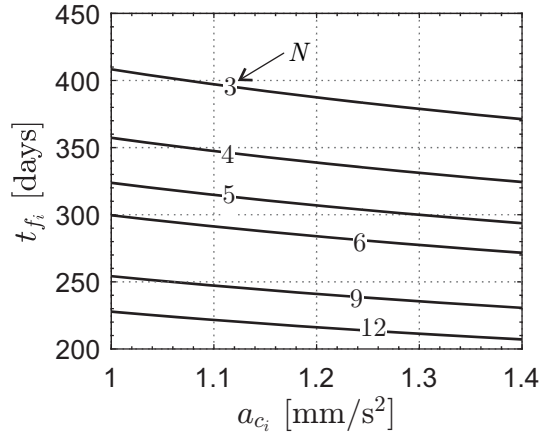

(b) $a_c = 1\,\mathrm{mm/s^2}$

Figure 5. Time required to accomplish an arc of the constellation deployment mission $t_{f_i} = t_{f_i}(a_{c_i}, N)$ when $a_c = \{0.1, 1\}\,\mathrm{mm/s^2}$.

Table 2. Constellation deployment performance as a function of N when $a_c = 1\,\mathrm{mm/s^2}$.

$\Delta\theta_{B_i}$ [deg]	N	t_f [days]
120	3	785
90	4	1030
72	5	1241
60	6	1438
40	9	1953
30	12	2407

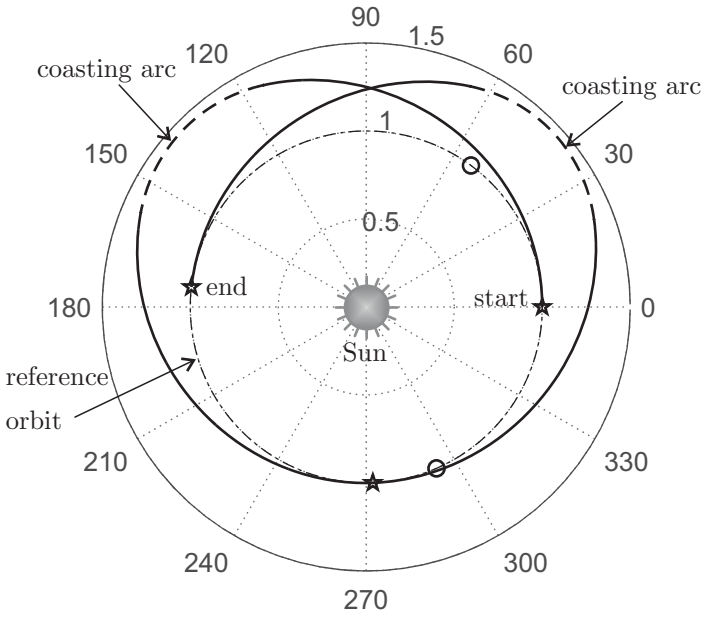

Figure 6. Constellation deployment trajectory with $a_c = 1\,\mathrm{mm/s^2}$ and $N = 3$ (propelled arc: solid line; coasting arc: dash line; satellite releases: stars; deployed satellite position at t_f: circles).

5. Conclusions

This work has presented a preliminary analysis of an optimal phasing maneuver along a circular heliocentric orbit performed by means of an Electric Solar Wind Sail. Because such a propulsive system allows its thrust to be generated without the need of any propellant consumption, time-optimal phasing trajectories have been investigated in both cases of drift ahead and drift behind maneuvers. For a given (fixed) angular displacement, a drift behind maneuver is the most convenient option in terms of required time.

A special application of phasing maneuvers has been proposed, which consists in a constellation deployment scenario by means of a deployer spacecraft. The simulation results suggest that a constellation of equally-spaced satellites could be inserted along the Earth's heliocentric orbit by a deployer propelled by an electric sail, even though the total required time becomes reasonable only using a medium- or high-performance E-sail configuration.

Acknowledgments

This work is supported by the University of Pisa, Progetti di Ricerca di Ateneo (Grant no. PRA 2018 44).

References

[1] Howard, M., "Project Helios," *Spaceflight*, Vol. 17, No. 5, 1975, pp. 184–188.

[2] Chipman, E., "Overview of NASA solar physics programs," *Proceedings of SPIE - The International Society for Optical Engineering*, Vol. 184, 1979, pp. 256–263. doi:10.1117/12.957459.

[3] Acton, L., Tsuneta, S., Ogawara, Y., et al., "The Yohkoh mission for high-energy solar physics," *Science*, Vol. 258, No. 5082, 1992, pp. 618–625. doi:10.1126/science.258.5082.618.

[4] Wenzel, K.-P., Mardsen, R. G., Page, D. E., and Smith, E. J., "Ulysses: The first high-latitude heliospheric mission," *Advances in Space Research*, Vol. 9, No. 4, 1989, pp. 25–29. doi:10.1016/0273-1177(89)90089-6.

[5] Phillips, J. L., Bame, S. J., and Barnes, A., "Ulysses solar wind plasma observation from pole to pole," *Geophysical Research Letters*, Vol. 22, No. 23, 1995, pp. 3301–3304. doi:10.1029/95GL03094.

[6] Roberts, C. E., "Long term mission at the Sun-Earth libration point L1: ACE, SOHO, and WIND," *Advances in the Astronautical Sciences*, Vol. 142, 2012, pp. 1263–1282.

[7] Stone, E. C., Frandsen, A. M., Mewaldt, R. A., Christian, E. R., Margolies, D., Ormes, J. F., and Snow, F., "The Advanced Composition Explorer," *Space Science Reviews*, Vol. 86, No. 1–4, 1998, pp. 1–22.

[8] Franz, H., Sharer, P. J., Ogilvie, K., and Desch, M., "WIND nominal mission performance and extended mission design," *AIAA/AAS Astrodynamics Specialist Conference and Exhibit*, Boston, MA, USA, 1998. doi:10.2514/6.1998-4467.

[9] Dunham, D. W., Jen, S. J., Roberts, C. E., Seacord, A. W., Sharer, P. J., Folta, D. C., and Muhonen, D. P., "Transfer Trajectory Design for the SOHO Libration-Point Mission," *43rd International Astronautical Congress*, Washington, DC, USA, 1992.

[10] Vulpetti, G., Circi, C., and Pino, T., "Coronal Mass Ejection early-warning mission by solar-photon sailcraft," *Acta Astronautica*, Vol. 140, 2017, pp. 113–125. doi:10.1016/j.actaastro.2017.07.042.

[11] Niccolai, L., Quarta, A. A., and Mengali, G., "Electric sail elliptic displaced orbit with advanced thrust model," *Acta Astronautica*, Vol. 138, 2017, pp. 503–511. doi:10.1016/j.actaastro.2016.10.036.

[12] Niccolai, L., Quarta, A. A., and Mengali, G., "Electric sail-based displaced orbits with a refined thrust model," *Proceedings of the Institution of Mechanical Engineers, Part G: Journal of Aerospace Engineering*, Vol. 232, No. 3, 2018, pp. 423–432. doi:10.1177/0954410016679195.

[13] Szabo, A., "Flying into the Sun," *Nature Astronomy*, Vol. 2, No. 10, 2018, p. 829. doi:10.1038/s41550-018-0580-3.

[14] Kaiser, M. L., "The STEREO mission: An overview," *Advances in Space Research*, Vol. 36, No. 8, 2005, pp. 1483–1488. doi:10.1016/j.asr.2004.12.066.

[15] Mengali, G., and Quarta, A. A., "In-orbit repositioning of multiple solar sail spacecraft," *Aerospace Science and Technology*, Vol. 12, No. 7, 2008, pp. 506–514. doi:10.1016/j.ast.2007.12.003.

[16] Mengali, G., Quarta, A. A., and Aliasi, G., "Heliocentric phasing performance of electric sail spacecraft," *Acta Astronautica*, Vol. 127, 2016, pp. 474–481. doi:10.1016/j.actaastro.2016.06.033.

[17] Janhunen, P., "Electric sail for spacecraft propulsion," *Journal of Propulsion and Power*, Vol. 20, No. 4, 2004, pp. 763–764. doi:10.2514/1.8580.

[18] Huo, M., Mengali, G., and Quarta, A. A., "Electric Sail Thrust Model from a Geometrical Perspective," *Journal of Guidance, Control, and Dynamics*, Vol. 41, 2018, pp. 734–740. doi:10.2514/1.G003169.

[19] Clohessy, W., and Wiltshire, R., "Terminal Guidance System for Satellite Rendezvous," *Journal of the Aerospace Sciences*, Vol. 270, 1960, pp. 653–674.

[20] Mengali, G., Quarta, A. A., and Denti, E., "Relative motion of Sun-pointing Smart Dust in circular heliocentric orbits," *Journal of Guidance, Control, and Dynamics*, Vol. 41, No. 4, 2018, pp. 1009–1014. doi:10.2514/1.G003088.

[21] Quarta, A. A., and Mengali, G., "Minimum-time trajectories of electric sail with advanced thrust model," *Aerospace Science and Technology*, Vol. 55, 2016, pp. 419–430. doi:10.1016/j.ast.2016.06.020.

[22] Chobotov, V. A., *Orbital Mechanics*, 3rd ed., American Institute of Aeronautics and Astronautics, 2002, Chap. 7, pp. 152–155.

[23] Curtis, H. D., *Orbital Mechanics for Engineering Students*, Butterworth-Heinemann, 2014, Chap. 6, pp. 312–317.

[24] McInnes, C. R., "Azimuthal repositioning of payloads in heliocentric orbit using solar sails," *Journal of Guidance, Control, and Dynamics*, Vol. 26, No. 4, 2003, pp. 662–664. doi:10.2514/2.5098.

[25] Quarta, A. A., and Mengali, G., "Optimal solar sail phasing trajectories for circular orbit," *Journal of Guidance, Control, and Dynamics*, Vol. 36, No. 6, 2013, pp. 1821–1824. doi:10.2514/1.59372.

[26] Quarta, A. A., Mengali, G., and Denti, E., "Optimal in-orbit repositioning of Sun-pointing Smart Dust," *Acta Astronautica*, Vol. 154, 2019, pp. 278–285. doi:10.1016/j.actaastro.2018.03.036.

[27] Niccolai, L., Bassetto, M., Quarta, A. A., and Mengali, G., "A review of Smart Dust architecture, dynamics, and mission applications," *Progress in Aerospace Sciences*, Vol. 106, 2019, pp. 1–14. doi:10.1016/j.paerosci.2019.01.003.

[28] Niccolai, L., Anderlini, A., Mengali, G., and Quarta, A. A., "Impact of solar wind fluctuations on Electric Sail mission design," *Aerospace Science and Technology*, Vol. 82–83, 2018, pp. 38–45. doi:10.1016/j.ast.2018.08.032.

[29] Toivanen, P. K., and Janhunen, P., "Electric sailing under observed solar wind conditions," *Astrophysics and Space Sciences Transactions*, Vol. 5, No. 1, 2009, pp. 61–69. doi:10.5194/astra-5-61-2009.

[30] Bassetto, M., Mengali, G., and Quarta, A. A., "Thrust and torque vector characteristics of axially-symmetric E-sail," *Acta Astronautica*, Vol. 146, 2018, pp. 134–143.

[31] Bassetto, M., Mengali, G., and Quarta, A. A., "Attitude dynamics of an electric sail model with a realistic shape," *Acta Astronautica*, Vol. 159, 2019, pp. 250–257. doi:10.1016/j.actaastro.2019.03.064.

[32] Bassetto, M., Mengali, G., and Quarta, A. A., "Stability and Control of Spinning Elecric Solar Wind Sail in Heliostationary Orbit," *Journal of Guidance, Control and Dynamics*, Vol. 42, No. 2, 2019, pp. 425–431. doi:10.2514/1.G003788.

[33] Bryson, A. E., and Ho, Y. C., *Applied Optimal Control*, Hemisphere Publishing Corporation, 1975, Chap. 2, pp. 71–89.

[34] Lawden, D. F., *Optimal Trajectories for Space Navigation*, Butterworths & Co., London, 1963, pp. 54–60.

[35] Shampine, L. F., and Gordon, M. K., *Computer Solution of Ordinary Differential Equations: The Initial Value Problem*, W. H. Freeman & Co Ltd, San Francisco, 1975, Chap. 10. ISBN: 0-716-70461-7.

[36] Shampine, L. F., and Reichelt, M. W., "The MATLAB ODE Suite," *SIAM Journal on Scientific Computing*, Vol. 18, No. 1, 1997, pp. 1–22. doi:10.1137/S1064827594276424.

[37] Janhunen, P., Quarta, A. A., and Mengali, G., "Electric solar wind sail mass budget model," *Geoscientific Instrumentation, Methods and Data Systems*, Vol. 2, No. 1, 2013, pp. 85–95. doi:10.5194/gi-2-85-2013.